Electronic Supplementary Information

Cu nanocluster Loaded TiO_2 Nanosheets for Highly-Efficient Generation of CO-Free Hydrogen by Selective Photocatalytic Dehydrogenation of Methanol to Formaldehyde

Fengyang Yu,[†] Liyong Chen,*[†] Xuezhao Li,[†] Xiaoshuang Shen,[§] He Zhao,[‖] Chunying Duan[†] and Qianwang Chen*[‡]

[†]State Key Laboratory of Fine Chemicals, Dalian University of Technology, Dalian, 116024, P. R. China.

[‡]Hefei National Laboratory for Physical Science at Microscale, Department of Materials Science & Engineering, University of Science and Technology of China, Hefei, 230026, P. R. China.

[§]School of Physical Science & Technology, Yangzhou University, Yangzhou, 225002, P. R. China.

[‖]Division of Chemistry, Dalian University of Technology, Dalian, 116024, P. R. China.

*Corresponding author.

Email: lychen@dlut.edu.cm (L. Chen), cqw@ustc.edu.cn (Q. Chen)

Experimental Section

Chemicals and Characterization Methods

All chemical reagents were used as received. Chemicals of tetrabutyl titanate ($Ti(OBu)_4$, 98%), copper acetate ($Cu(Ac)_2 \cdot H_2O$), trimesic acid, anhydrous methanol, hydrofluoric acid (HF, 40 *wt*%) were purchased from Sinopharm Chemical Reagent Co., Ltd, China.

The microstructure and morphology observations of samples were performed with transmission electron microscope (TEM) of Tecnai F30 operated at 300 kV, scanning electron microscope (SEM) of HITACHI UHR FE-SEM SU8220, and a JEOL JEM-ARM200F microscope with spherical aberration (Cs) correction at an accelerating voltage of 200 kV. X-ray diffraction (XRD) was conducted in a Rigaku D/Max 2400 automatic powder X-ray diffractometer with Cu-*K*α radiation (λ = 1.5418 Å). The content of element was evaluated by inductively coupled plasma atomic emission spectroscopy (ICP-AES) on Optima 2000DV. X-ray photoelectron spectroscopy (XPS) was collected on Thermo ESCALAB 250Xi with Al-*K*α radiation (*hv* = 1486.6 eV). Electrochemical/photoelectrochemical measurements were carried out on a CHI660C electrochemical workstation with a conventional three-electrode cell. Electrochemical impedance spectroscopy (EIS) was collected on a ZAHNER ENNIUM electrochemical workstation with a conventional three-electrode cell at room temperature in Ar atmosphere. UV-Vis absorption spectroscopy was measured on a HITACHI U-4100 spectrometer. Electron spin resonance (ESR) spectrum was conducted on Bruker A200 at room temperature.

Preparation of Sample for ICP Test

In a typical procedure, catalyst (5 mg) was carefully added into a 15 mL-Teflon-lined autoclave containing the mixed acid of hydrofluoric acid (49%, 1 mL) and nitric acid (68%, 1 mL), and heated at 120 °C for 4 h to form a transparent solution. Deionized water (5 mL) was carefully added the autoclave. Afterwards, the mixture was transferred to 50-mL volumetric flask to make a uniform and diluted solution (50 mL) by careful adding of deionized water.

Density Functional Theory (DFT) Calculations

The present first principle calculations are performed with the projector augmented wave (PAW) method based on DFT (Phys. Rev. B, 1994, 50, 17953-17979). The exchange-functional is treated using the generalized gradient approximation (GGA) of Perdew-Burke-Ernzerhof (PBE) functional (Phys. Rev. Lett., 1996, 77, 3865-3868; Phys. Rev. B, 1999, 59, 1758-1775). The cut-off energy of the plane-wave basis is set at 400 eV for optimize calculations of atoms optimization. The vacuum spacing in a direction perpendicular to the plane of the catalyst is at least 10 Å. The Brillouin zone integration is performed using 3×3×1 Monkhorst and Pack k-point sampling for TiO_2(001). The self-consistent calculations apply a convergence energy threshold of

10^{-6} eV. The maximum Hellmann-Feynman force for each ionic optimization step is 0.05 eV/Å. In addition, spin polarizations is also considered in all calculations. Finally, the free energy can be obtained by including the zero point energy (ZPE) and the entropy (S) corrections in equation G = Eads-EZPE-TS, The EZPE could be obtained from the calculation of vibrational frequencies for the adsorbed species.

Apparent surface charge concentration

The apparent surface charge concentration was determined in accordance to the equation:

$$\frac{1}{C^2} = \frac{2}{q\varepsilon\varepsilon_0 N_d}(E - E_{fb} - \frac{k_b T}{q}), \qquad 3$$

where C, k_b, T, E, E_{fb}, N_d, and q represent space charge capacitance, Boltzmann's constant, absolute temperature, applied potential, flat-band potential, surface charge density, and electronic charge respectively; ε, ε_0 are dielectric constant of semiconductor and permittivity in vacuum, respectively.

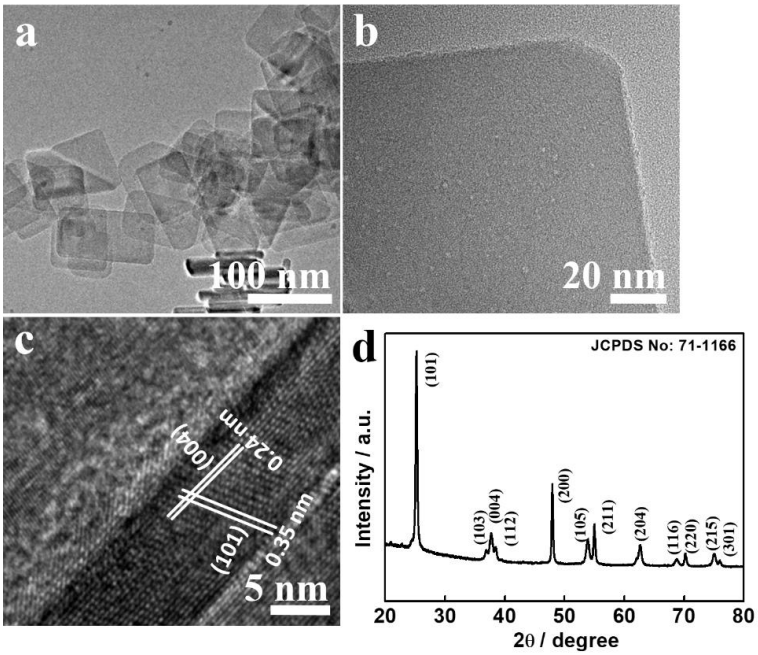

Figure S1. (a and b) different magnified TEM images, and (c) HRTEM image of vertical TiO_2 nanosheets treated at 450 ^oC in air; (d) XRD pattern of the treated TiO_2 nanosheets at 450 ^oC in air.

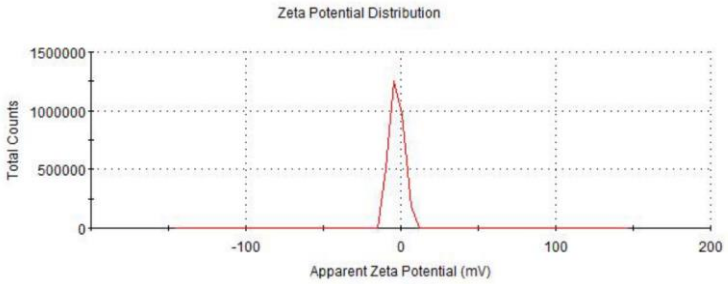

Figure S2. Zeta potential of the treated TiO_2 nanosheets at 450 ºC in air.

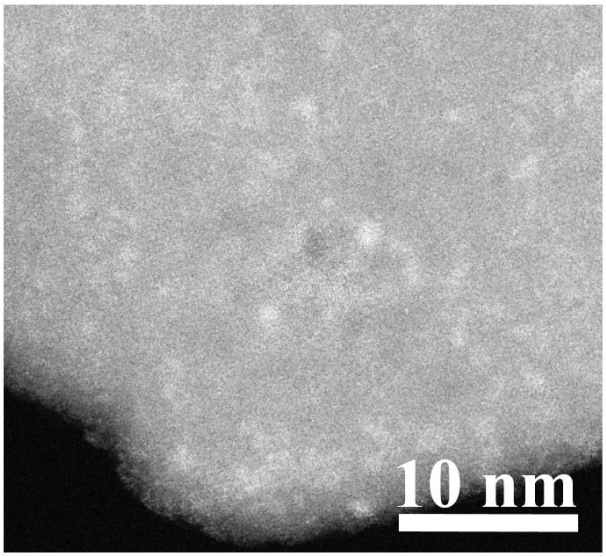

Figure S3. HAADF-STEM image of TiO_2/Cu_50 heterostructures.

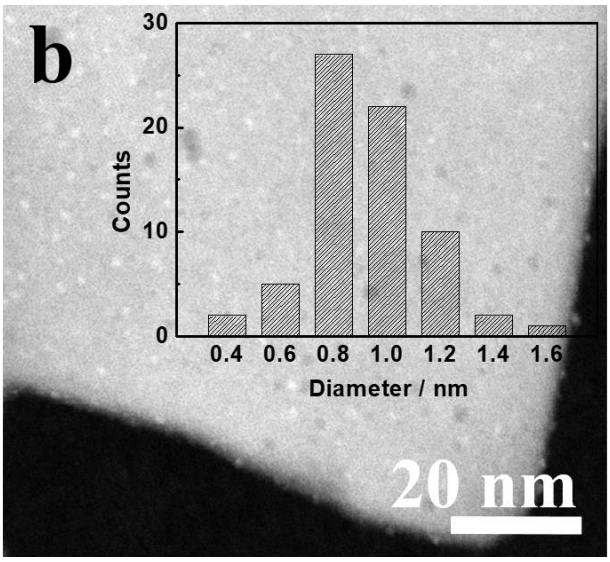

Figure S4. Size distribution of Cu nanoclusters.

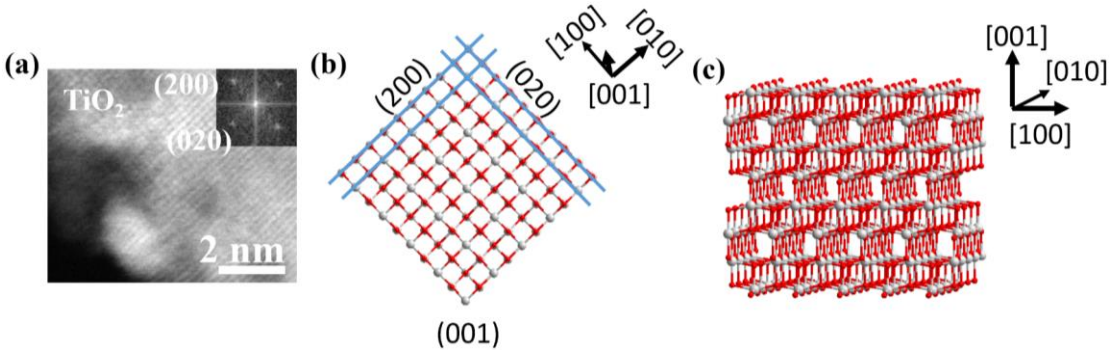

Figure S5. (a) High resolution STEM image of TiO_2/Cu_50, and (b, c) Schematic illustrating surface structures of TiO_2 nanosheet corresponding to (001) facets. Inset of (a) is a selected-area electron diffraction pattern obtained from the fast-Fourier-transform-filtered high-resolution STEM image.

On the basis of Weiss zone law, the direction of crystal axis [uvw] can be calculated by equations of $u = k_1 \cdot l_2 - k_2 \cdot l_1$, $v = l_1 \cdot h_2 - l_2 \cdot h_1$, and $w = h_1 \cdot k_2 - h_2 \cdot k_1$, wherein $(h_1k_1l_1)$ and $(h_2k_2l_2)$ are corresponding to two intersecting crystal planes. Therefore, the selected-area electron diffraction pattern is indexed as the [001] zone axis diffraction, indicating that the top and bottom surfaces of the nanosheets are the (001) planes. That is, the exposed crystal plane is the (001) facet, which is orderly stacked along the plane of paper.

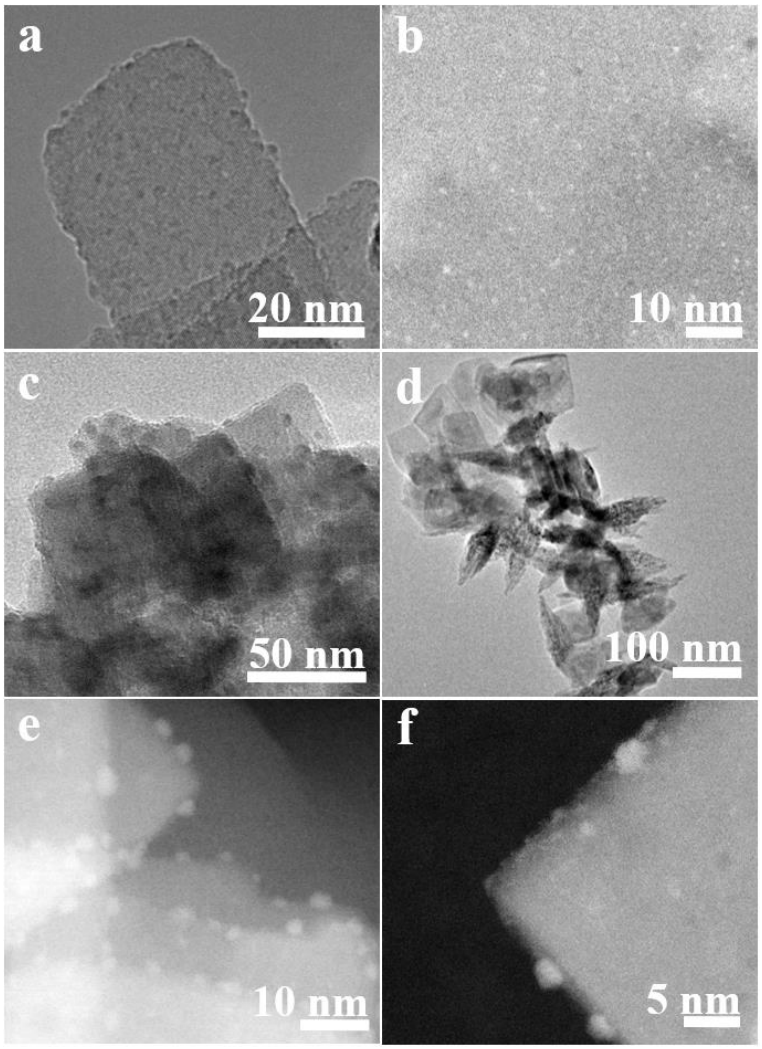

Figure S6. (a) TEM and (b) HAADF-STEM images of TiO_2/Cu_20; (c, d) TEM and (e, f) HAADF-STEM images of TiO_2/Cu_100.

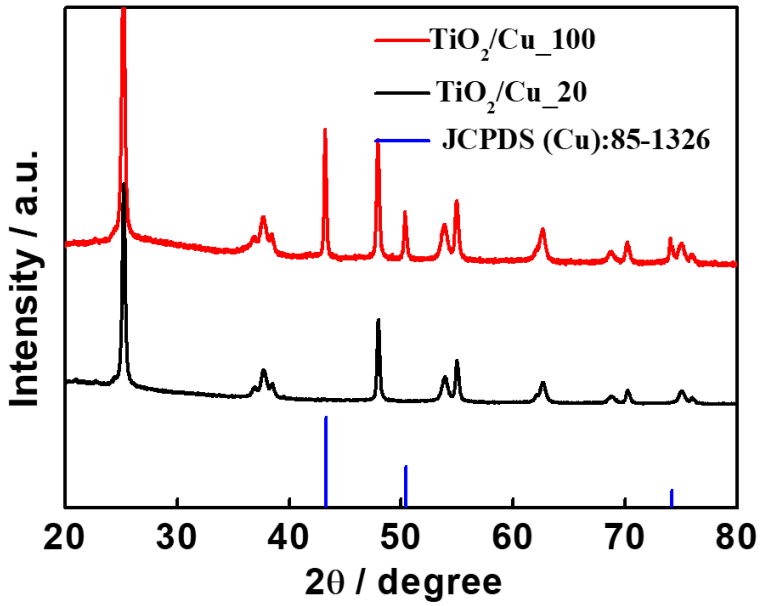

Figure S7. XRD patterns of TiO_2/Cu_20 and _100.

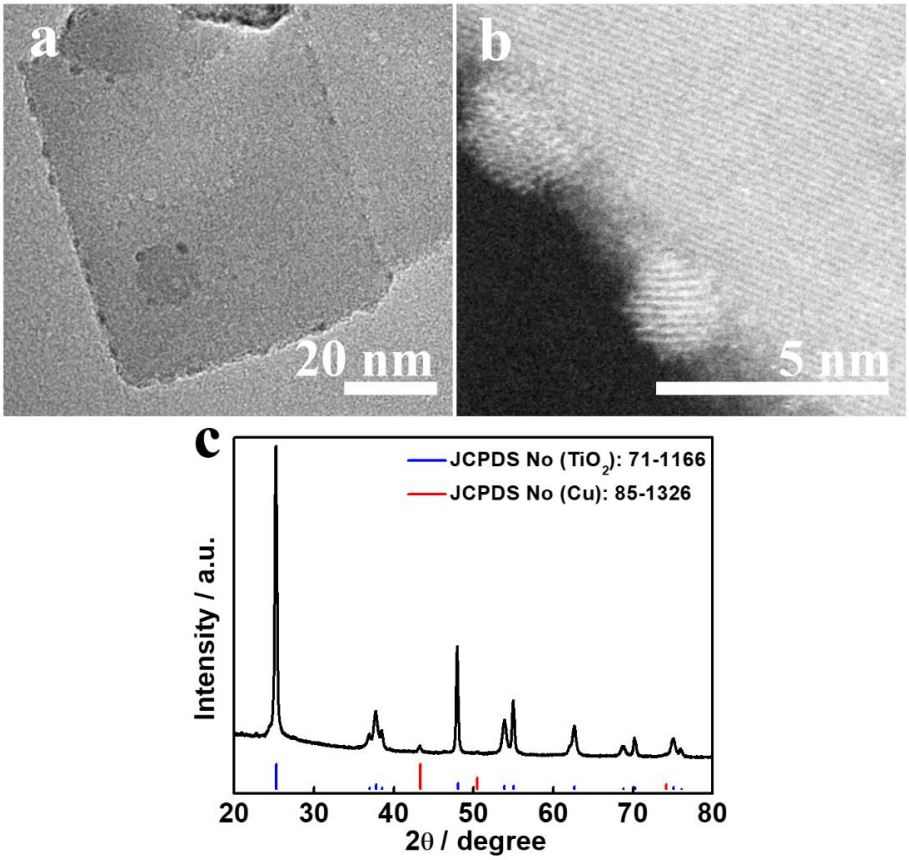

Figure S8. (a) TEM and (b) STEM images and (c) XRD pattern of TiO_2/Cu_50_*d*.

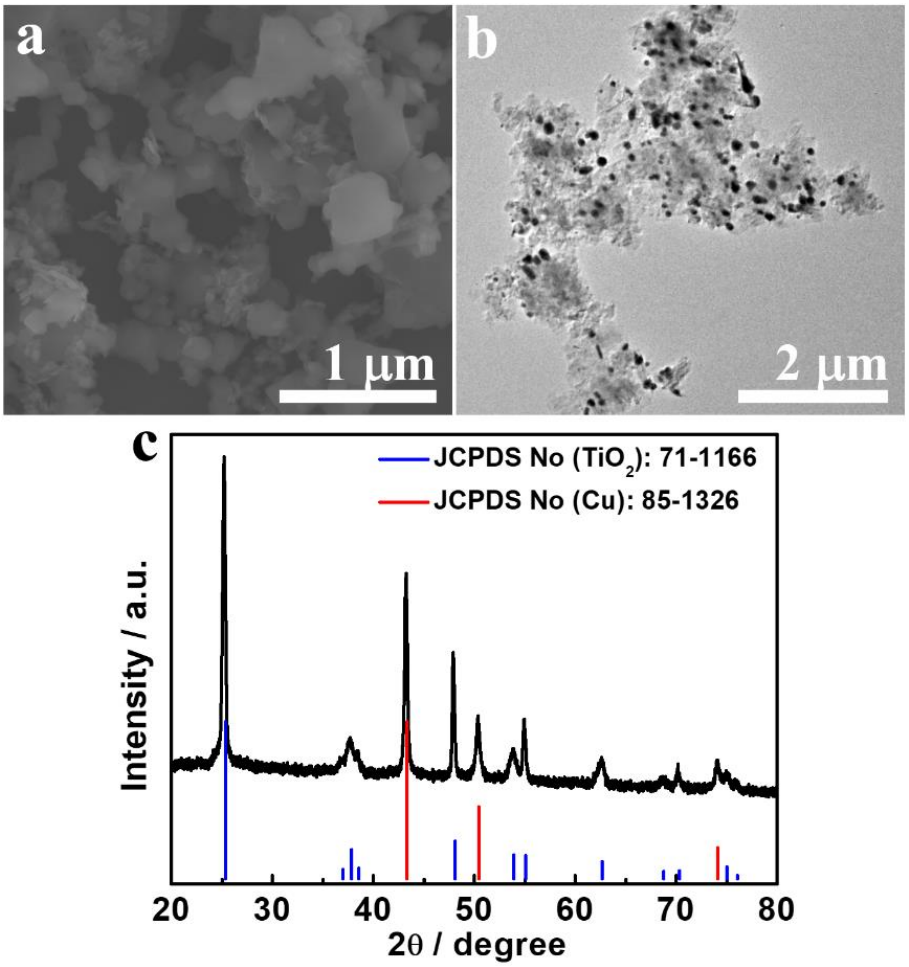

Figure S9. (a) SEM and (b) TEM images and (c) XRD pattern of sample.
The as-prepared sample by thermal treatment of TiO_2/HKUST-1 that was synthesized by a solvothermal reaction of TiO_2 nanosheets in a methanol/water solution of $Cu(Ac)_2 \cdot H_2O$ and trimesic acid.

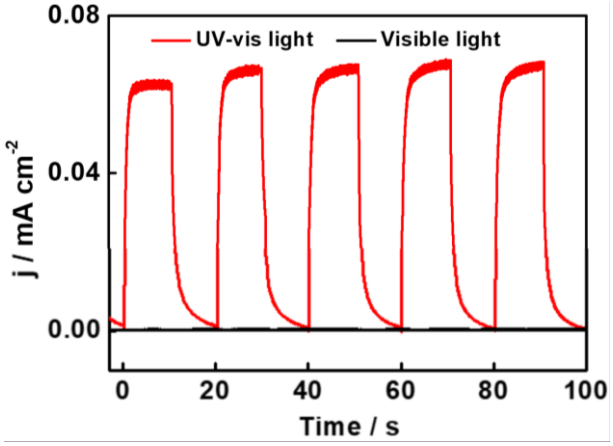

Figure S10. Photocurrent density comparison of TiO_2/Cu_50 under light irradiation of different wavelength ranges.

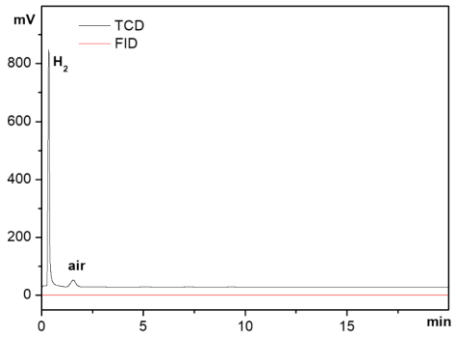

Figure S11. Gas products of CH_3OH dehydrogenation over TiO_2/Cu_50 upon UV-visible light irradiation for 1 h by GC analysis.

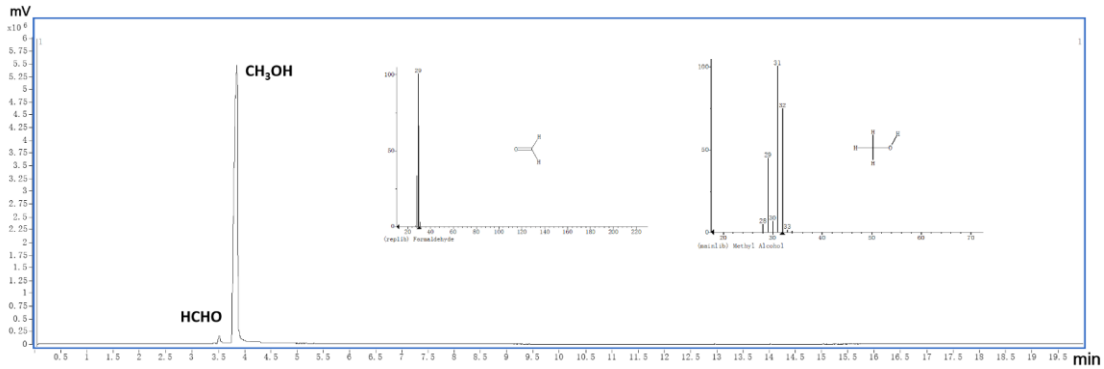

Figure S12. Liquid products of CH_3OH dehydrogenation over TiO_2/Cu_50 upon UV-visible light irradiation for 1 h by GC analysis. Insets are the mass spectra of liquids.

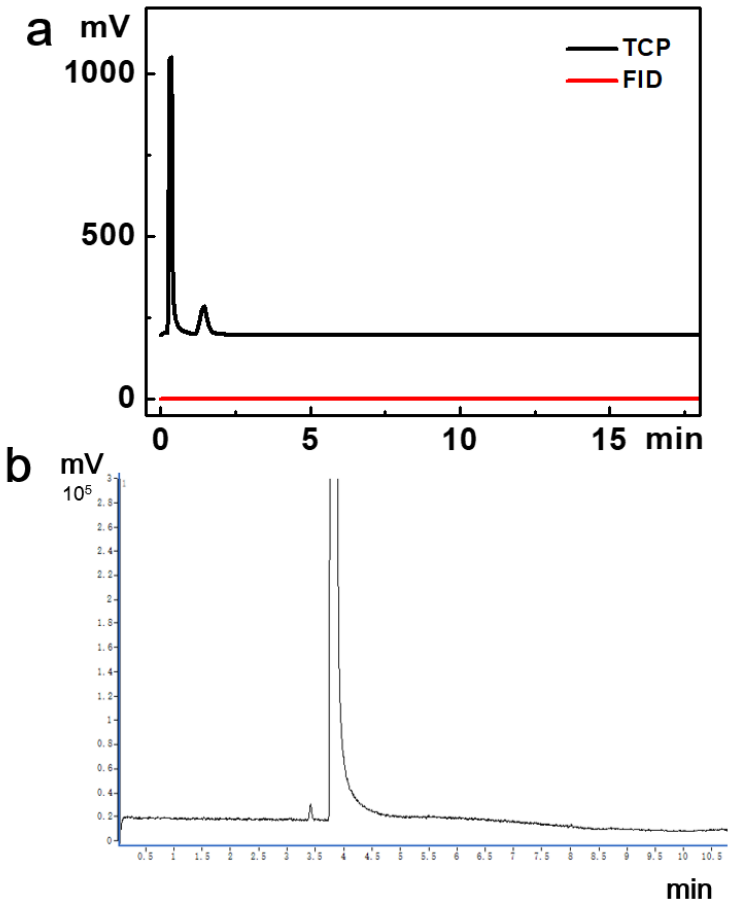

Figure S13. CH_3OH dehydrogenation TiO_2/Cu_50 upon UV-visible light irradiation for 4 h: (a) Gas products and (b) liquid products detected by GC.

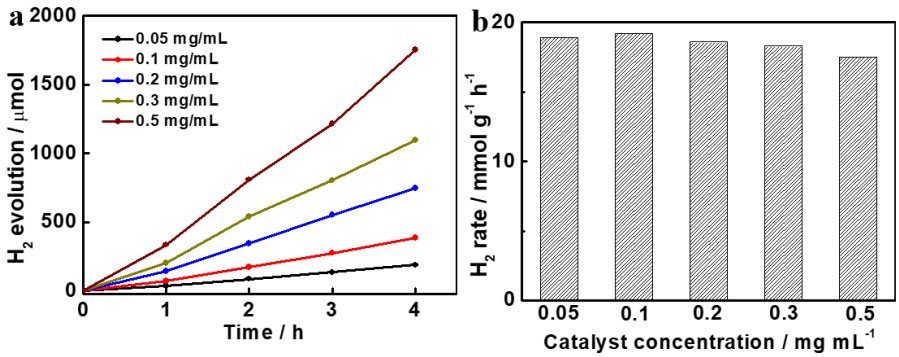

Figure 14. Photocatalytic tests of TiO_2/Cu_50 with different concentrations in photocatalytic system: (a) the amount of hydrogen and (b) the hydrogen evolution rate.

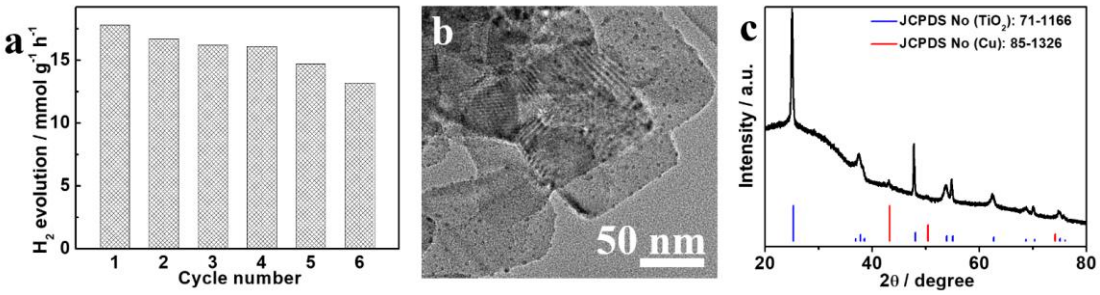

Figure S15. (a) Recyclability tests of TiO_2/Cu_50 for the catalytic dehydrogenation of CH_3OH, and (b) TEM image and (c) XRD pattern of the used TiO_2/Cu_50 via six-cycle reaction.

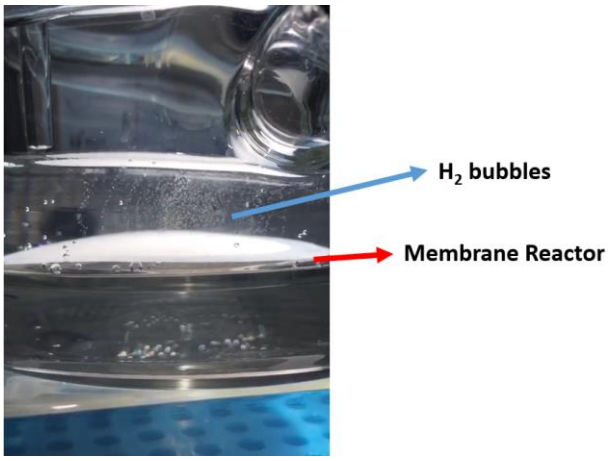

Figure S16. The optical photo of a membrane reactor upon irradiation of a 300 W Xe lamp (~350 mW cm^{-2}).

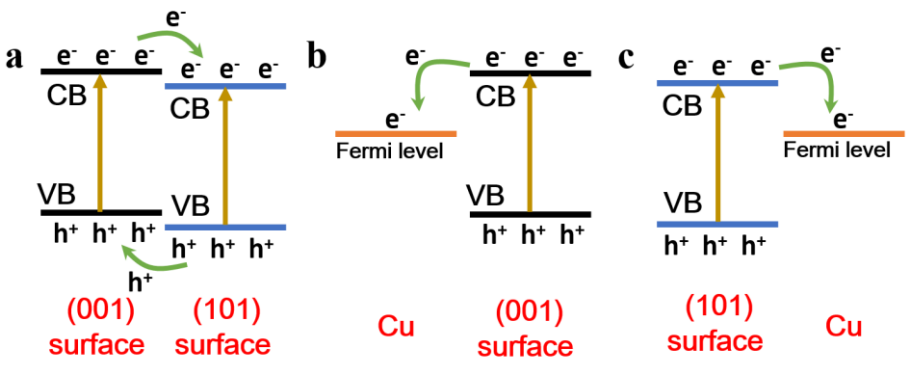

Figure 17. Schematic illustrating various heterojunctions of (a) TiO_2(001)-TiO_2(101), (b) TiO_2(001)-Cu, and (c) TiO_2(101)-Cu in TiO_2/Cu for the separation of photogenerated charge carriers.

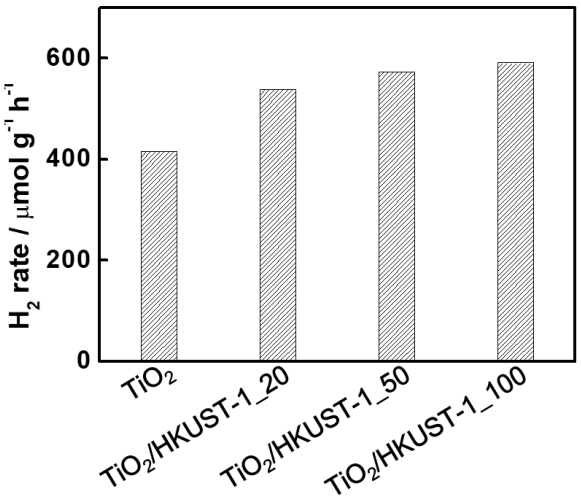

Figure 18. TiO_2 and various TiO_2/HKUST-1 photocatalytic tests of CH_3OH dehydrogenation under UV-visible light irradiation for 4 h.

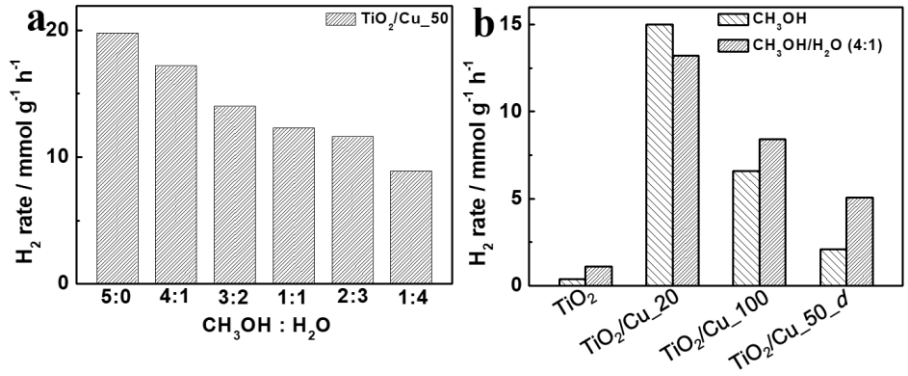

Figure S19. Photocatalytic tests: (a) TiO_2/Cu_50 in different photocatalytic systems under UV-visible light irradiation for 4 h, and (b) different photocatalysts in different photocatalytic systems upon irradiation of UV-visible light for 4 h.

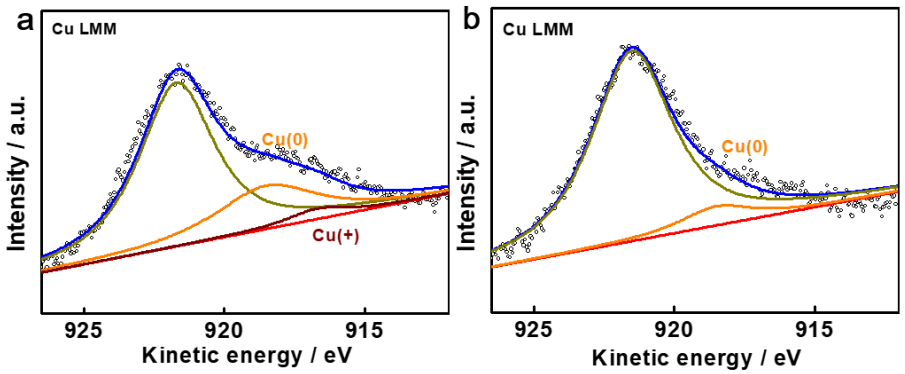

Figure S20. Cu LMM Auger spectra of (a) TiO_2/Cu_50 and (b) TiO_2/Cu_50_*d*. Owing to the presence of interference peak of Ti2s at 921.7 eV, high background can greatly affect the observation of Cu LMM from both catalysts.

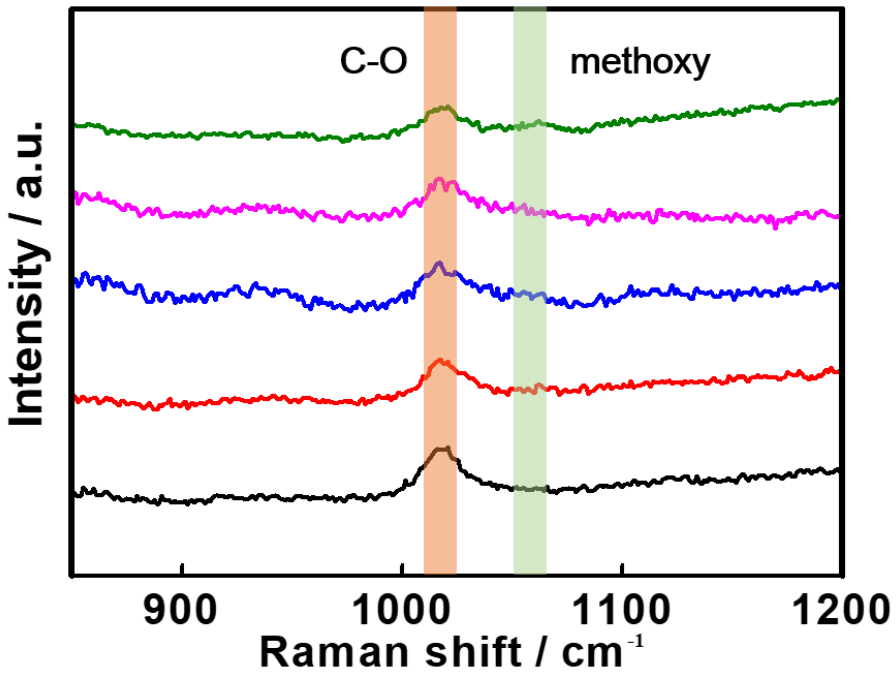

Figure S21. In-situ Raman spectra of the dehydrogenation of CH_3OH.
In detail, a 10 μL suspension prepared by adding of TiO_2/Cu_50 into water is taken to disperse on carbon paper (0.5 cm × 0.5 cm), the dried electron is fixed in a home-made three-electrode device for photocatalytic dehydrogenation of methanol at 1.4 V versus Ag/AgCl.

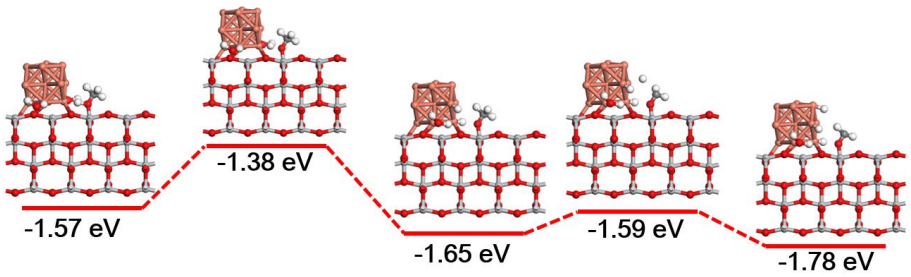

Figure S22. Free energy pathways of CH_3OH adsorption and CH_3OH dissociation process on Cu nanocluster loaded $TiO_2(001)$ in H_2O/CH_3OH system.

Table S1. Atomic percentage of Cu, Ti and O in various catalysts TiO_2/Cu_*n*.

	Cu (at.%)	Ti (at.%)	O (at.%)
TiO_2/Cu_20	0.67	34.82	64.51
TiO_2/Cu_50	1.26	34.01	64.73
TiO_2/Cu_100	2.19	33.89	63.92

Table S2. Flat-band potential and apparent electron carrier concentrations of the different catalysts

Catalyst	Flat-band potential E_{fb} (V, versus Ag/AgCl)	Apparent electron carrier density N_d (cm^{-3})
TiO_2	1.05	2.47×10^{19}
TiO_2/Cu_20	1.03	1.02×10^{20}
TiO_2/Cu_50	1.03	2.13×10^{20}
TiO_2/Cu_100	1.03	6.02×10^{19}
TiO_2/Cu_50_*d*	1.05	2.87×10^{19}

Table S3. Comparison of the photocatalytic activity in H_2 evolution on Cu or Cu compound modified TiO_2 photocatalysts.

Photocatalyst	Incident light (light intensity)	Catalytic medium	H_2 evolution rate (mmol g^{-1} h^{-1})	Quantum efficiency (%@wavelength)	Reference
Cu/TiO_2	300 W Xe lamp (80 mW cm^{-2})	10 % methanol	2.8	3.44@360 nm	[1]
Cu/TiO_2	4 × 3 W UV-LEDs (80 mW cm^{-2})	25% methanol	5.104	17.2@365 nm	[2]
CuO_x/TiO_2	300 W Xe lamp (80 mW cm^{-2})	20% methanol	1.523	7.05@365 nm	[3]
$Cu(OH)_2/TiO_2$	4 × 3 W UV-LEDs (80 mW cm^{-2})	ethylene glycol (0.09 M)	3.418	13.9@360 nm	[4]
Cu_2O/TiO_2	500 W Xe lamp (3.6 mW cm^{-2})	10 % methanol	2.442	4.32@365 nm	[5]
Cu/TiO_2	300 W Xe lamp (–)	10 % methanol	12.779	–	[6]
Cu/TiO_2	300 W Xe lamp (–)	20% methanol	6.046	–	[7]
$Cu/CuO/TiO_2$	300 W Xe lamp (–)	25% methanol	0.851	–	[8]
CuO_x/TiO_2	50 W Xe lamp (–)	20%	0.1126	–	[9]
Cu/TiO_2	300 W Xe lamp (100 mW cm^{-2})	methanol	17.8	16.4@365 nm	this work

Table S4. Comparison of the photocatalytic activity in H_2 evolution on different photocatalysts toward methanol.

Photocatalyst	Incident light (light intensity)	Catalytic medium	H_2 evolution rate (mmol g^{-1} h^{-1})	Quantum efficiency (%@wavelength)	Product	Reference
MgO	1000 W Hg lamp (388 mW cm^{-2})	methanol	0.32	–	H_2, HCHO	[10]
Trans-$[Fe^{II}(apH)_2(MeOH)_2]$	200 W Hg–Xe lamp (–)	methanol	1.34 (mol mol^{-1} h^{-1})	4.8@289±10 nm	H_2, HCHO	[11]
Au/TiO_2	150 W halogen lamp (100 mW cm^{-2})	methanol	1.503	–	H_2, HCHO	[12]
Ni/CdS	300 W Xe lamp (150 mW cm^{-2})	methanol	48.2	photon-to-hydrogen efficiency 95@405 nm	H_2, HCHO, CH_4, CO, CO_2	[13]
Cu/TiO_2	300 W Xe lamp (100 mW cm^{-2})	methanol	17.8	19@365 nm	H_2, HCHO	this work

References

(1) Tian, H.; Zhang, X. L.; Scott, J.; Ng, C.; Amal, R. TiO_2-Supported Copper Nanoparticles Prepared via Ion Exchange for Photocatalytic Hydrogen Production. *J. Mater. Chem. A* **2014,** *2* (18), 6432–6438.

(2) Xiao, S.; Liu, P.; Zhu, W.; Li, G.; Zhang, D.; Li, H. Copper Nanowires: A Substitute for Noble Metals to Enhance Photocatalytic H_2 Generation. *Nano Lett.* **2015,** *15* (8), 4853–4858.

(3) Liu, Y.; Zhang, B.; Luo, L.; Chen, X.; Wang, Z.; Wu, E.; Su, D.; Huang, W. TiO_2/Cu_2O Core/Ultrathin Shell Nanorods as Efficient and Stable Photocatalysts for Water Reduction. *Angew. Chem. Int. Ed.* **2015,** *54* (50), 15260–15265.

(4) Yu, J.; Ran, J. Facile Preparation and Enhanced Photocatalytic H_2 Production Activity of $Cu(OH)_2$ Cluster Modified TiO_2. *Energ. Environ. Sci.* **2011,** *4* (4), 1364–1371.

(5) Li, Y.; Wang, B.; Liu, S.; Duan, X.; Hukey, Z. Synthesis and Characterization of Cu_2O/TiO_2 Photocatalysts for H_2 Evolution from Aqueous Solution with Different Scavengers. *Appl. Surf. Sci.* **2015,** *324*, 736–744.

(6) Foo, W. J.; Zhang, C.; Ho, G. W. Non-Noble Metal Cu-Loaded TiO_2 for Enhanced Photocatalytic H_2 Production. *Nanoscale* **2013,** *5* (2), 759–764.

(7) Zhu, J.; Xiong, J.; Cheng, G.; Li, W.; Dou, S. Promoting Solar-to-Hydrogen Evolution on Schottky Interface with Mesoporous TiO_2-Cu Hybrid Nanostructures. *J. Colloid. Interf. Sci.* **2019,** *545*, 116–127.

(8) Hou, H.; Shang, M.; Gao, F.; Wang, L.; Liu, Q.; Zheng, J.; Yang, Z.; Yang, W. Highly Efficient Photocatalytic Hydrogen Evolution in Ternary Hybrid TiO_2/CuO/Cu Thoroughly Mesoporous Nanofibers. *ACS Appl. Mater. Interfaces* **2016,** *8* (31), 20128–20137.

(9) Yang, F.; Liu, M.; Chen, X.; Xu, Z.; Zhao, H. Simultaneous Control over Lattice Doping and Nanocluster Modification of a Hybrid CuO_x/TiO_2 Photocatalyst during Flame Synthesis for Enhancing Hydrogen Evolution. *Sol. RRL* **2018,** *2* (12), 1800215.

(10) Liu, Z.; Yin, Z.; Cox, C.; Bosman, M.; Qian, X.; Li, N.; Zhao, H.; Du, Y.; Li, J.; Nocera, D. G. Room Temperature Stable CO_x-Free H_2 Production from Methanol with Magnesium Oxide Nanophotocatalysts. *Sci. Adv.* **2016,** *2* (9), e1501425.

(11) Wakizaka, M.; Matsumoto, T.; Tanaka, R.; Chang, H.-C. Dehydrogenation of Anhydrous Methanol at Room Temperature by o-Aminophenol-Based Photocatalysts. *Nat. Commun.* **2016,** *7*, 12333.

(12) Liu, B.; Louis, M.; Jin, L.; Li, G.; He, J. Co-Template Directed Synthesis of Gold Nanoparticles in Mesoporous Titanium Dioxide. *Chem. Eur. J.* **2018,** *24* (38), 9651–9657.

(13) Huang, H.; Jin, Y.; Chai, Z.; Gu, X.; Liang, Y.; Li, Q.; Liu, H.; Jiang, H.; Xu, D. Surface Charge-Induced Activation of Ni-Loaded CdS for Efficient and Robust Photocatalytic Dehydrogenation of Methanol. *Appl. Catal. B-Environ.* **2019,** *257*, 117869.